Applied Surface Science 510 (2020) 144804

Contents lists available at ScienceDirect

Applied Surface Science

journal homepage: www.elsevier.com/locate/apsusc

Full Length Article

The role of oxide formation on insulating versus metallic substrates during Co and Ru selective ALD

Steven Wolf[a], Michael Breeden[a], Scott Ueda[a], Jacob Woodruff[c], Mansour Moinpour[c], Ravindra Kanjolia[c], Andrew Kummel[a,b,*]

[a] Materials Science and Engineering Program, University of California, San Diego, La Jolla, CA 92093, United States
[b] Department of Chemistry and Biochemistry, University of California, San Diego, La Jolla, CA 92093, United States
[c] EMD Performance Materials, Haverhill, MA 01832, United States

ARTICLE INFO

Keywords:
ALD
Cobalt
Ruthenium
Bottom-up fill
Organometallic
XPS

ABSTRACT

Advanced interconnect materials replacing Cu include Co and Ru, particularly at early metallization steps in small vias where Cu resistivity increases due to grain boundary scattering. In this study, hyper-selective Co ALD was performed from Bis(1,4-di-tert-butyl-1,3-diazadienyl) cobalt [$Co(dad)_2$] and two co-reactants (formic acid [HCOOH] and tert-butylamine [TBA]). Utilizing HCOOH, *in situ* XPS showed no deposition on an insulator (SiO_2) and thick films on metallic substrates (Pt) consistent with infinite selectivity; however, Cu etching was observed. By switching to TBA, similar thick Co films were achieved on Cu with no evidence of etching; while only 4% CoO_x on SiO_2 was observed consistent with Co scavenging weakly bound oxygen from under-coordinated sites. This scavenging produced to an unreactive oxidic particulate. These co-reactants were also employed with a Ru precursor: η^4-2,3-dimethylbutadiene ruthenium tricarbonyl [$RuDMBD(CO)_3$]. Selective deposition on metals vs. SiO_2 with sub-1 nm roughness in AFM was achieved; however, the formation of sub-stoichiometric RuO_x on SiO_2 was unable to inhibit further deposition due to the low valency of the $RuDMBD(CO)_3$ precursor and Ru not oxidizing as easily as Co. The results revealed a robust type of passivant-free metal ALD that can be self-limiting on oxides if the metal is able to fully oxidize.

1. Introduction

As the scaling of transistors continues, so does the need for depositing conductive interconnect metal in shrinking vias. It is desired to have selective metal deposition on metals against insulators for bottom-up fill for both middle-of-line (MOL or MEOL) and back end-of-line (BEOL) processing. This would induce the formation and growth of larger grains, which are expected to decrease via and interconnect resistance by reducing grain boundaries and decreasing surface roughness (see Fig. 1). This scattering has been well documented and simulated for current Cu interconnects [1–3]. In addition, bottom-up atomic layer deposition (ALD) growth is the preferred deposition method since it should prevent keyhole and seam formation in tight geometries and high aspect ratio features. The key advanced metals for bottom-up growth include cobalt [4] and ruthenium [5]. Cobalt is particularly important since it used as both a capping layer on Cu to protect it from oxidation [6], and in sub-10 nm vias, where Co is considered to be a better conductor than Cu due to Co having a smaller electron mean free path. Additionally, there are problems with Cu electroplating in sub-10 nm vias [7,8].

Conductive Co has previously been reported by the Winter group and was grown via ALD using Bis(1,4-di-tert-butyl-1,3-diazadienyl) cobalt [$Co(dad)_2$] and either formic acid (HCOOH) or tert-butylamine (TBA) at temperatures near 180 °C with high selectivity on metals versus insulators but were not studied with *in situ* XPS [9,10]. Additionally, the mechanism of selectivity was presumed to be precursor decomposition by catalysis on metallic surfaces. Other recent work involving $Co(dad)_2$ was performed by Kim *et al* who used ozone as a co-reactant, but was only able to achieve cobalt oxide films at 120 °C [11]. Ozone as a co-reactant is corrosive to Cu interconnects [12,13]; therefore, exploring and discovering co-reactants that are not caustic to Cu are crucial. This study seeks to understand the mechanism for ALD Co and Ru selectivity on metals versus insulators using *in situ* XPS, and ultimately determine the role of oxide formation on insulators that results in infinite selectivity.

Additionally, the co-reactants TBA and HCOOH were applied to ALD with a Ru precursor, η^4-2,3-dimethylbutadiene ruthenium tricarbonyl [$RuDMBD(CO)_3$]. Previous reports show that this precursor can react with O_2 and plasma O_2 at elevated temperatures (> 220 °C) to form ruthenium metal or ruthenium oxide depending on the temperature and

* Corresponding author.

https://doi.org/10.1016/j.apsusc.2019.144804
Received 18 May 2019; Received in revised form 17 November 2019; Accepted 19 November 2019
Available online 14 December 2019

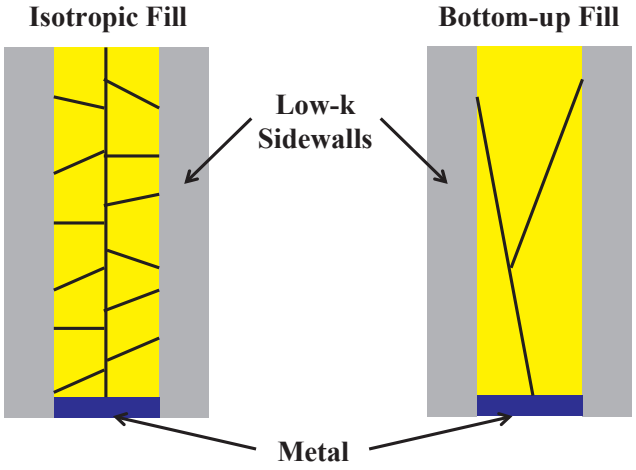

Fig. 1. Selective bottom-up Co. By depositing Co selectively on metals vs. low-k materials during via fill, bottom-up growth can induce the formation of larger grains that provide lower electrical resistance.

amount of oxygen dosed per cycle [14]. Additionally, resistivities of these films were reported as low as 13.7 μohm-cm after a post-deposition anneal [15]. More recent work has also seen ALD using $RuDMBD(CO)_3$ with H_2O at lower temperatures [16], but no reference to selective deposition has been reported. Khan *et al* have used dicarbonyl-bis(5-methyl-2,4-hexanediketonato)Ru and O_2 at 283 °C to selectively deposit Ru; however, the use of an inhibitor was necessary to achieve about 10 nm of selectivity [17]. In the present study, the authors are reporting a novel selective Ru ALD that has been achieved on metals vs. insulating substrates as function of controlling the temperature and by using HCOOH or TBA as a co-reactant.

2. Experimental methodology

ALD cobalt metal was explored using a metal-organic cobalt precursor, $[Co(dad)_2]$, and either a co-reactant of HCOOH or TBA at 180 °C on Cu, Pt, and SiO_2 substrates. Similarly Ru, films were deposited at temperatures between 100 °C and 325 °C with HCOOH and TBA to determine the selectivity window. The deposited Co films were studied using *in situ* x-ray photoelectron spectroscopy (XPS) and atomic force microscopy (AFM). Cross-sectional scanning electron microscopy (SEM) was used to check the film thicknesses to estimate a growth per cycle.

Cu and Pt samples used in this study were deposited by DC magnetron sputtering on SiO_2 substrates consisting of 300 nm of thermal SiO_2 on Si(0 0 1) (University Wafer). Samples underwent an *ex situ* degrease involving rinses in acetone, methanol, and water before being rapidly loaded into the vacuum chamber (< 5 min). Once loaded into the load lock chamber, the samples were transferred into the UHV XPS chamber and typically heated to 350 °C for 30 min to produce clean starting substrates. Precursor exposures were performed in a deposition chamber, as shown in Fig. 2. The deposition chamber and dosing lines were pumped with a turbomolecular pump producing a base pressure of $\sim 5 \times 10^{-7}$ Torr. The chamber was heated ~125 °C, and dosing lines were kept ~10–20 °C warmer than precursor containers to ensure precursors would not condense in the lines. The $Co(dad)_2$ precursor was heated to 150 °C and was used with ultrahigh purity N_2 that was passed through a purifier to act as a push gas for the delivery of the $Co(dad)_2$ to the samples. $RuDMBD(CO)_3$ was supplied by EMD and gently heated to 30 °C. TBA and HCOOH (Sigma Aldrich) were used as received and dosed at room temperature. No purge gas was employed to reduce any surface contamination/oxygen incorporation into the films. Before moving samples into the deposition chamber, they were preheated in the UHV chamber via a pyrolytic boron nitride heater. For the ALD, samples were heated via an enclosed cartridge heater to eliminate hot wire reactions and minimize CVD, which would lead to improved selectivity. After deposition, samples were transferred back to the UHV chamber where *in situ* x-ray photoelectron spectroscopy (XPS) was performed without breaking vacuum. A monochromatic XPS system (Al kα $h\nu$ = 1486.7 eV) was employed to collect surface-sensitive spectra at an angle of 30° with respect to the surface parallel. An electron pass energy of 50 eV and a line width of 0.1 eV were used for collection, and CASA XPS v.2.3 utilizing Shirley background subtractions was used for analysis. Relative sensitivity factors (Schofield) were used to correct raw peak areas before normalization to the sum of all components present during the collected scan. In addition to XPS, surface topography was characterized with AFM and samples thick enough were analyzed with cross-sectional SEM.

3. Hyper-selective Co ALD

3.1. Deposition with HCOOH

Nearly infinite selective deposition of Co on a conductor and not an SiO_2 was observed for 180 °C ALD with $Co(dad)_2$ and HCOOH. Fig. 3 plots the XPS corrected peak areas normalized to the sum of all components after 100 ALD cycles followed by an additional 100 cycles on UHV annealed Pt vs SiO_2. Note all raw XPS data can be found in the supplemental materials. Pt was employed since it is not etched by HCOOH. On Pt, a thick (> 10 nm) Co^{+0} film was deposited while virtually no deposition occurred on SiO_2. The raw binding energy peaks of the Co spectra on Pt and SiO_2 are plotted in Fig. 3C and 3D, respectively. The metallic Co $2p_{3/2}$ signal on Pt had a binding energy of ~778 eV consistent with previous reports for metallic Co [18,19], while there was no detectable Co 2p signal on SiO_2 after deposition.

AFM images showed no change on SiO_2 before and after Co ALD cycles consistent with no nuclei formation, while the Co on Pt surface roughness remains below 1.8 nm (Fig. 4). The brighter white-colored dots observed on SiO_2 before and after deposition did not significantly change and can be attributed to hydrocarbon contamination from ambient exposure; these features were ~2–3 nm tall before and after deposition. On Pt, the imaging indicated a low density of pits consistent with depositing Co on a significant carbon component as seen in XPS; plasma pre-clean should eliminate these features by reducing the carbon on the starting surface allowing for better nucleation and growth.

To verify self-limiting precursor exposures consistent with ALD, a saturation study was performed and monitored with XPS; Fig. 5A highlights the effect of individual additional half cycle amounts that resulted in self-limiting $Co(dad)_2$ and HCOOH exposures confirming ALD behavior. Essentially, 1 pulse (1 s exposure) of each precursor was followed by 2 additional pulses of the same precursor (2 s) to confirm self-limiting behavior in XPS peak areas. Additionally, this study revealed a novel mechanism about the reaction. Previously it was thought that the HCOOH dissociatively chemisorbed to produce atomic H which removed the ligands from $Co(dad)_2$. Instead, XPS indicated that HCOOH did not remove the ligands but instead induced a ligand-exchange process. Fig. 5B shows the Co 2p peaks that indicated the HCOOH induced a higher binding energy component consistent with a formate on the surface that was subsequently removed upon exposure to $Co(dad)_2$. The Co $2p_{3/2}$ and the Co $2p_{1/2}$ shifted components appear at about 786 eV and 797 eV, respectively. Note that the Co $2p_{3/2}$ component is slightly less distinguishable due to electron scattering on the high intensity peak. Fig. 5C verifies the presence of the formate on the surface; a higher BE C 1 s peak forms after HCOOH deposition at ~288.5 eV. Similarly, this peak is removed upon exposure to $Co(dad)_2$.

3.2. Selective Co from TBA

Deposition with HCOOH was attempted on Cu substrates (Fig. 6A); however, the Cu substrate signal never decreased to zero, consistent

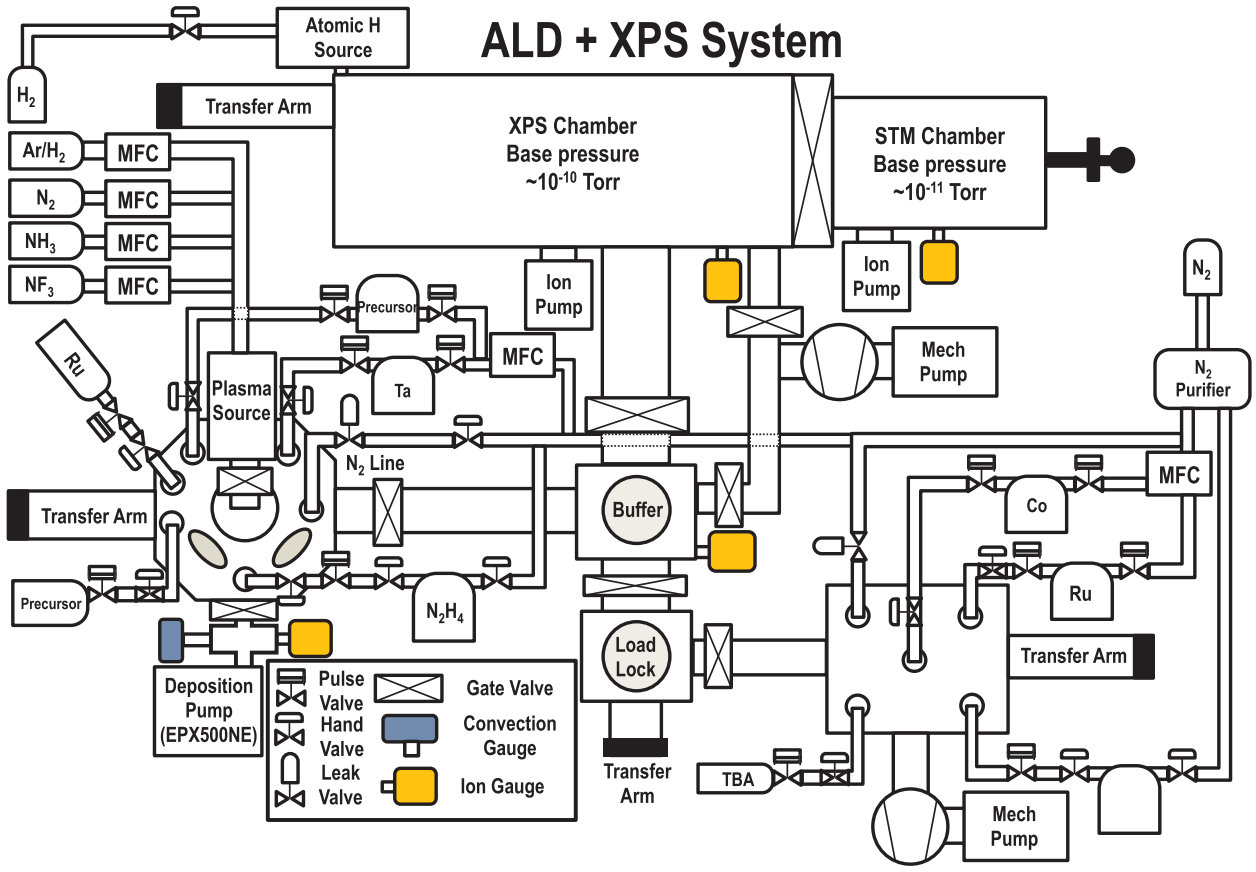

Fig. 2. Chamber schematic. An ALD chamber connected *in situ* to the XPS system allows for chemical composition characterization without exposure to ambient conditions. Additionally, a second chamber with an RF downstream plasma source can be used to clean samples with atomic hydrogen.

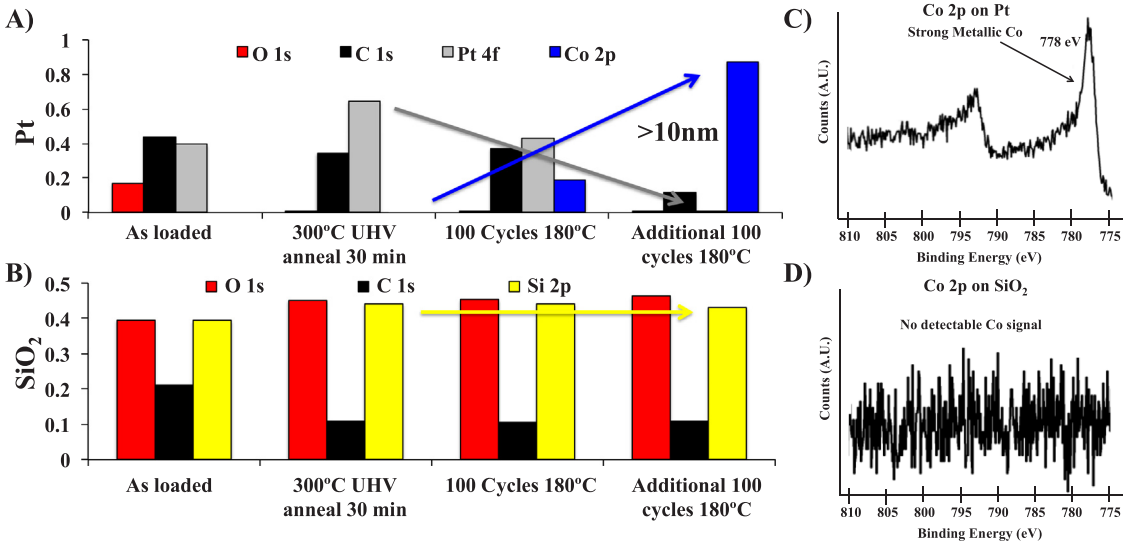

Fig. 3. XPS of UHV annealed substrates that underwent 100 + 100 additional ALD cycles of $Co(dad)_2$ + HCOOH at 180 °C. (A) On Pt, a completely buried Pt signal was consistent with a film > 10 nm thick. The rapid decrease in the Pt signal (grey) was consistent with a conformal film. (B) On SiO_2, the constant Si signal and lack of a Co signal indicated no Co consistent with infinite selectivity. Raw XPS Co 2p spectra showed a strong metallic component on (C) Pt, while no observable spectra is observed on (D) SiO_2.

with either etching of the substrate [20,21] or etching of the depositing Co film by HCOOH. Both etching mechanisms would prevent full attenuation of the underlying Cu substrate by an overlayer Co film. Therefore, an alkyl amine co-reactant (TBA) was also studied (Fig. 6B). For $Co(dad)_2$ + TBA ALD at 180 °C, reduced Co metal films were deposited on Cu and Pt substrates with hyper-selectivity against SiO_2. Films as thick as 30 nm were grown on the conductors while completely attenuating the substrate Cu 2p peaks consistent with zero etching of Cu. On SiO_2, only 4% CoO_x was deposited after an initial 50 ALD cycles. After an additional 250 ALD cycles, there was still only 4% CoO_x indicative of saturation and hyper-selectivity due to a self-limiting growth on the oxide (Fig. 7B). The Co $2p_{3/2}$ signal on SiO_2 was highly shifted in

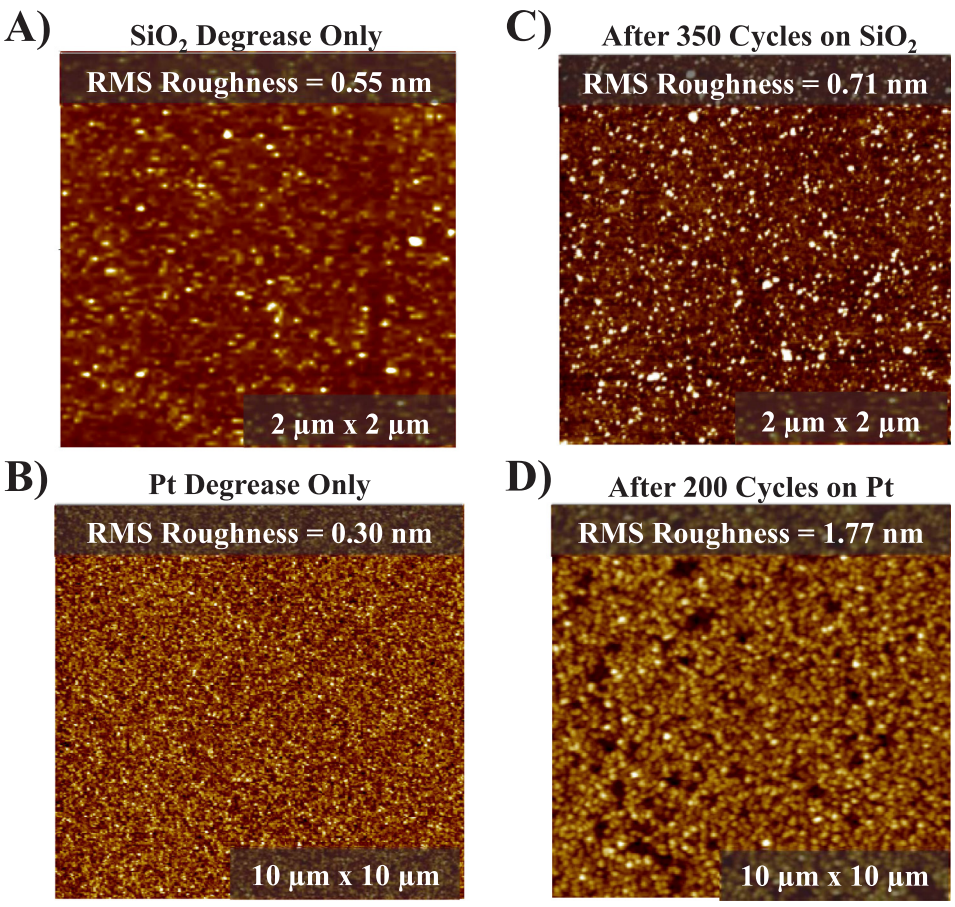

Fig. 4. AFM imaging before and after ALD cycles on SiO_2 and Pt. On SiO_2, (A) before a degrease and (C) after cycles, no significant change was observed, while on Pt (B) before and (D) after deposition surface roughness increased from 0.30 nm to 1.77 nm. Note there was carbon on the starting Pt surface; therefore, plasma cleaning Pt should allow for a more uniform Co film.

comparison to the signal on Cu (Fig. 7C and D). This shifted signal on SiO_2 had a peak position at ~782 eV, corresponding to a very oxygen rich, and likely stoichiometric Co_2O_3 or Co_3O_4 [22,23]. It should be noted that the SiO_2 substrate can charge slightly in XPS, resulting in all peak positions being shifted including the overlayer Co peaks. Therefore correcting the peak positions of the Co 2p peaks relative to known Si and O_2 peak positions is necessary, which still results in a shifted Co peak. Additionally, after 300 total ALD cycles, there is no evidence of a metallic component allowing for the justification that CoO_x is being deposited on SiO_2. A similar saturation study for Co grown with TBA can be found in the supplemental materials.

AFM imaging and corresponding line trace data from 300 cycles of ALD with TBA confirmed smooth films with low surface roughness on Pt and Cu. After deposition on SiO_2, small (< 5 nm tall and ~5–10 nm wide) CoO_x particles were present on SiO_2 (Fig. 8), which corresponds to the CoO_x observed in the Co 2p XPS spectra.

To check for the bottom-up fill nature of Co using the TBA process, 3000 cycles of ALD was performed on a patterned sample from Applied Materials consisting of SiCOH/SiN sidewalls with Cu at the bottom of vias (Fig. 9). The patterned sample underwent a 300 °C atomic H clean

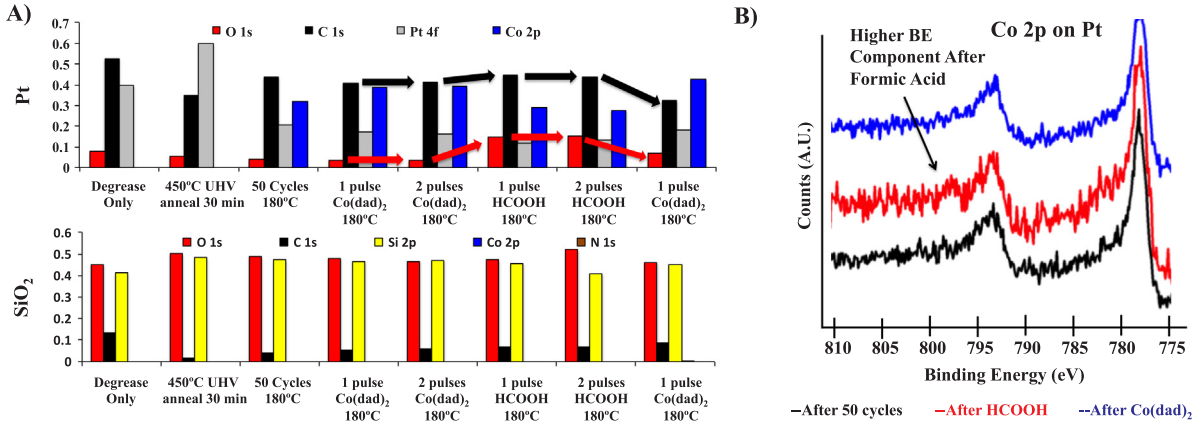

Fig. 5. Saturation study of $Co(dad)_2$ and HCOOH at 180 °C. (A) The self-limiting exposures were consistent with ALD. The C (black arrows) and O (red arrows) increased after HCOOH dosing suggested a formate was deposited on the surface. The decrease in C and O, and increase in Co, after $Co(dad)_2$ dosing indicated a ligand exchange mechanism for the reaction. After HCOOH dosing higher BE components in the (B) Co 2p spectrum and (C) C 1s spectrum are consistent with a formate deposited on the Co surface. The formate was removed after $Co(dad)_2$ dosing. (For interpretation of the references to colour in this figure legend, the reader is referred to the web version of this article.)

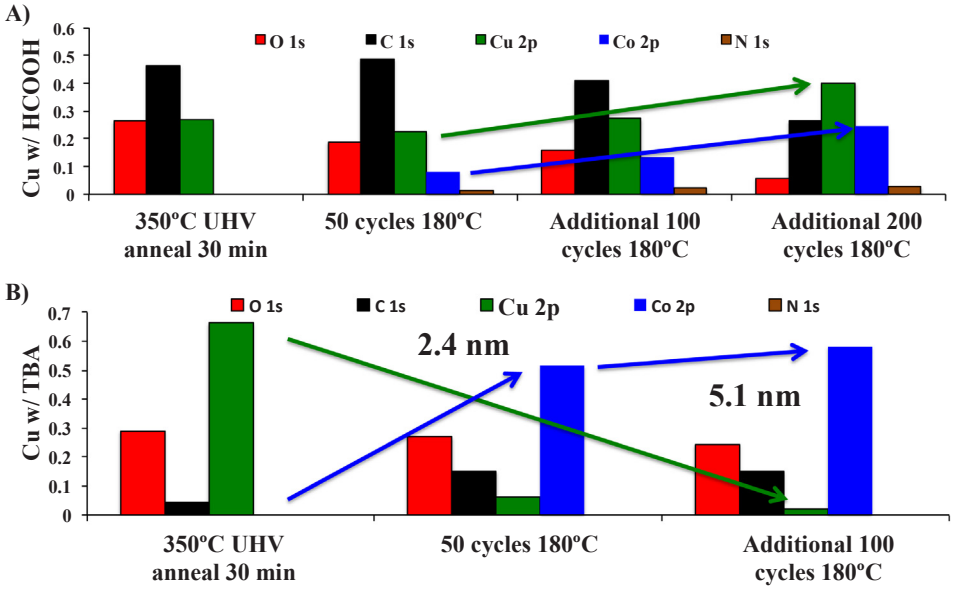

Fig. 6. Co ALD with $Co(dad)_2$ along with HCOOH vs TBA on Cu. (A) No attenuation of the substrate Cu signal (green arrow) with HCOOH was consistent with etching of Cu/CuO_x. (B) When ALD was performed with TBA, the Cu fully attenuation (green arrow) consistent with no etching. (For interpretation of the references to colour in this figure legend, the reader is referred to the web version of this article.)

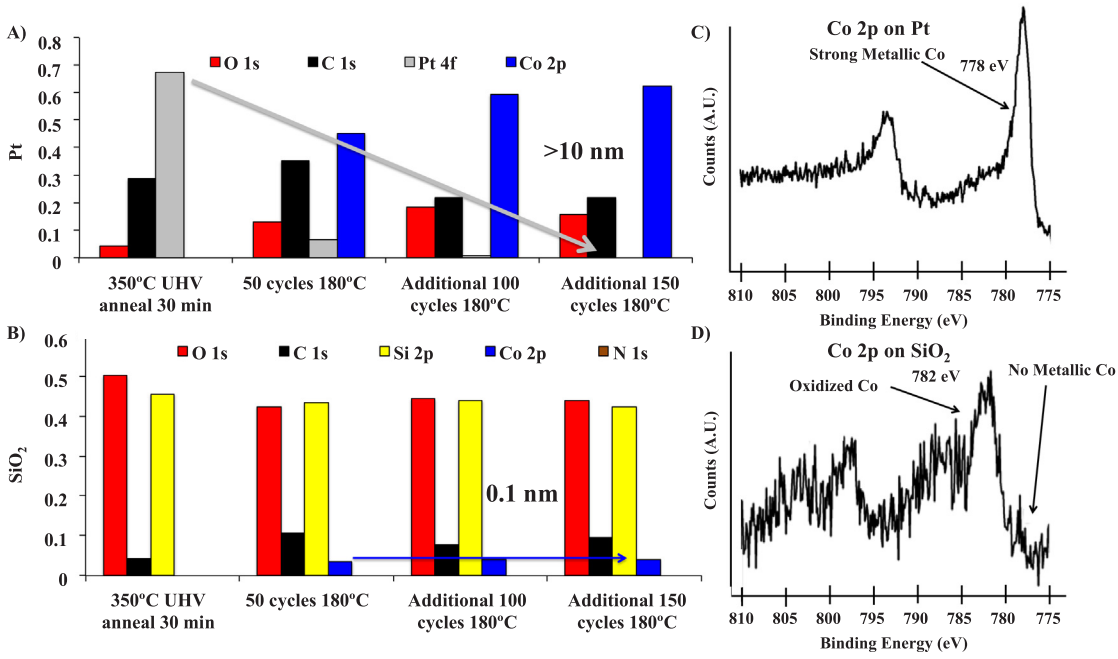

Fig. 7. Co ALD with $Co(dad)_2$ + TBA on Pt and SiO_2. (A) Attenuation of the substrate Pt signal (grey arrow) with TBA was consistent with growing a metallic film on Co from 300 cycles. (B) When ALD was performed with TBA on SiO_2, the SiO_2 showed a saturated amount of 4% CoO_x on the surface independent of the number of cycles (blue arrow). The Co 2p raw XPS spectra for growth on (C) Pt and (D) SiO_2 resulted in an ~4 eV difference in binding energy corresponding to metallic vs. oxidized Co deposition, respectively. (For interpretation of the references to colour in this figure legend, the reader is referred to the web version of this article.)

to ensure maximum cleanliness without damaging the low-k material. The amount of Cu on the patterned sample was < 1% (Fig. 9A) even by performing XPS analysis at 90°; however, the oxidation state was consistent with metallic Cu (shifted due to the effect of surface charging) after the H clean (Fig. 9B). The 3000 cycles of ALD was infinitely selective to the insulating SiCOH and SiN. Moreover, the cobalt began growing up from the metallic Cu. Approximately 12 nm of Co was grown bottom-up; however, the expected thickness was on the order of 100 nm. It was hypothesized that the porous SiCOH can poison the growth by allowing oxygen/water to diffuse out and oxidize the cobalt. Once oxidation occurs, further deposition was inhibited; therefore, metallic Co must be restored prior to additional deposition with this process. It should be noted that the atomic hydrogen clean was proven not to damage the SiCOH so it can be employed for the *in situ* clean.

4. Ru ALD

Ru metal ALD was performed with $RuDMBD(CO)_3$ and either HCOOH or TBA. It was observed that at a sample temperature of 325 °C, unselective growth of Ru was achieved on all surfaces. Likewise, when the sample temperature was set to 100 °C and the Ru ALD performed, there was no deposition. However, ALD at 215 °C resulted in selectivity of about 1.8 nm on Cu to 0.2 nm on SiO_2 when using TBA as a co-reactant. Further dropping the temperature to 200 °C resulted in slightly better selectivity, but decreased the growth rate by nearly a factor of four (Fig. 10). Similar selectivity was observed for HCOOH; however, similar to the Co ALD with HCOOH, AFM imaging after $RuDMBD(CO)_3$ and HCOOH showed rough films on Cu with an RMS surface roughness of nearly 10 nm consistent with etching. By using the

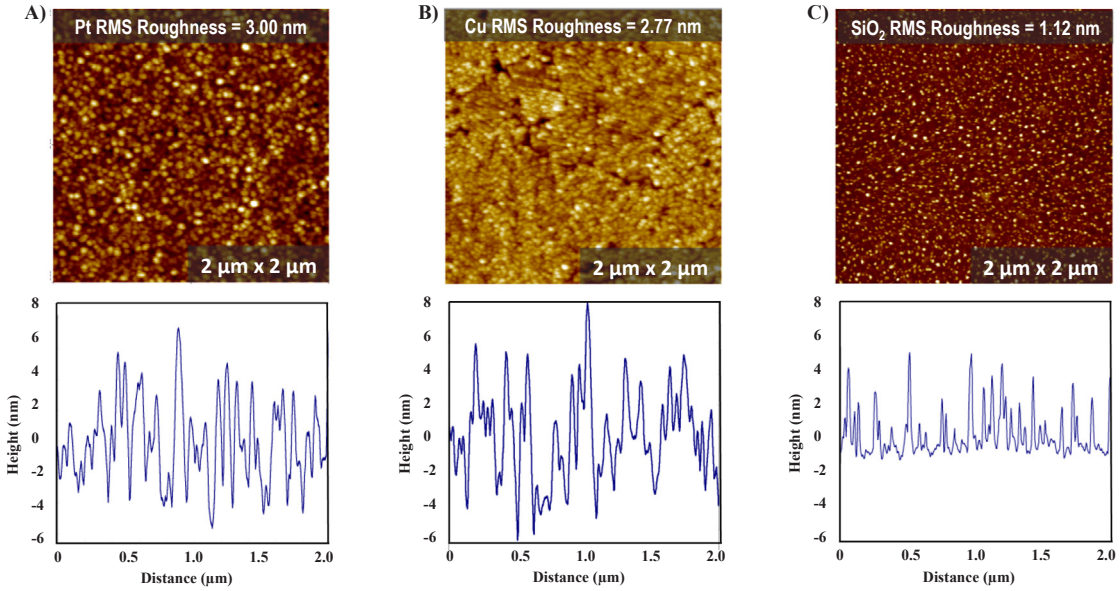

Fig. 8. Co AFM imaging and line traces of 300 cycles of ALD with $Co(dad)_2$ along with TBA on Pt, Cu, and SiO_2. (A) Pt and (B) Cu AFM imaging showed smooth films with low surface roughness. (C) Small nuclei consistent with the 4% CoO_x in XPS were detected on SiO_2. The nuclei on SiO_2 were about 2–5 nm tall and about 5–10 nm wide.

more-gentle TBA, the deposited films in AFM were very flat with a surface roughness of less than 1 nm consistent with the absence of etching (Fig. 11).

To understand the nature of the selectivity, the raw elemental Ru 3d peaks are plotted in Fig. 12. Fig. 12A shows the Ru 3d peak for deposition on SiO_2, while Fig. 12B shows the deposition on the conductors. It was observed that the Ru $3d_{5/2}$ peak had a position of ~280.3 eV for Ru grown on the oxide, whereas the peak position for growth on Pt and Cu was ~279.8 eV. These binding energies differ by only 0.5 eV; in the literature metallic Ru has been reported at values most commonly ranging from 279.9 eV to about 280.1 eV [24–26]. As for ruthenium oxides, values as high as ~283 eV have been reported for ruthenium in +3 and +4 oxidation states [26,27]. Observing a peak position nearly 2.5 eV lower than reported values for RuO_4 is more consistent with a metallic-like sub-stoichiometric RuO_x [27]. This very small shift coupled with the inability to achieve as high of a selectivity

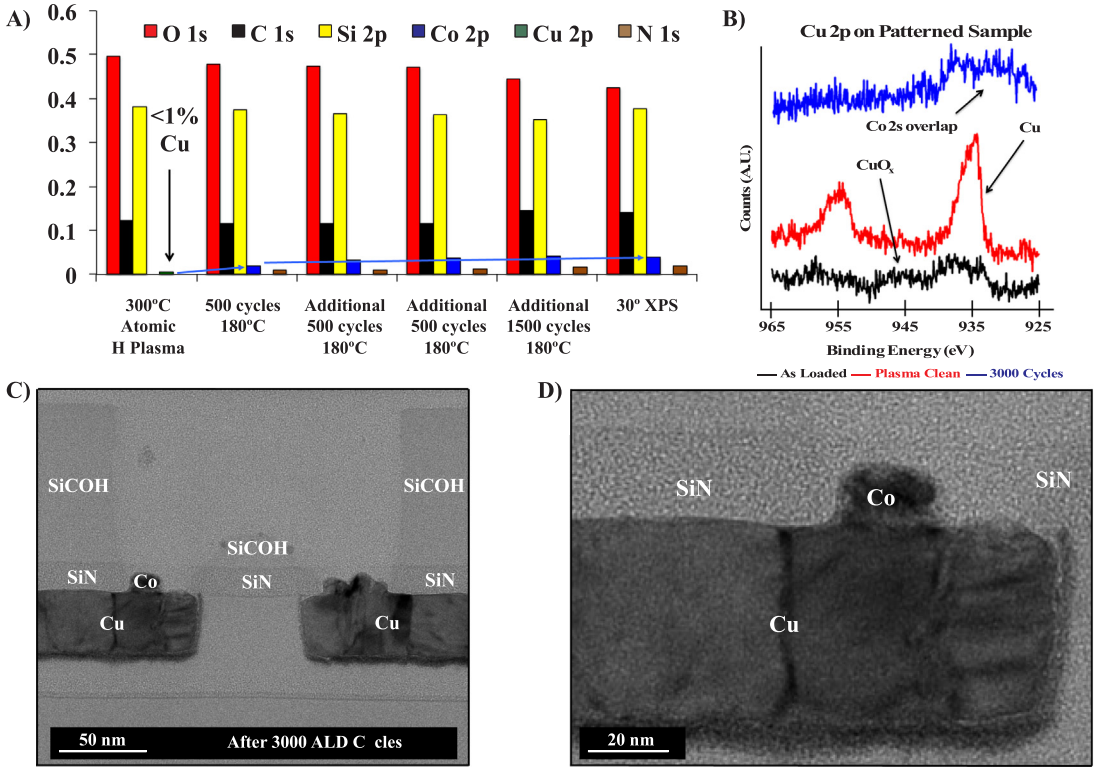

Fig. 9. Co XPS and TEM of 3000 cycles of ALD with TBA on patterned sample. (A) Normalized XPS data indicated Co grew after 500 cycles (blue arrow), but saturated after running additional cycles. (B) The Cu 2p peaks became metallic after plasma cleaning and buried after deposition. (C) ALD was selective for 3000 cycles against SiCOH and SiN. (D) Zoomed-in TEM highlighting ~12 nm Co grown on Cu surface.

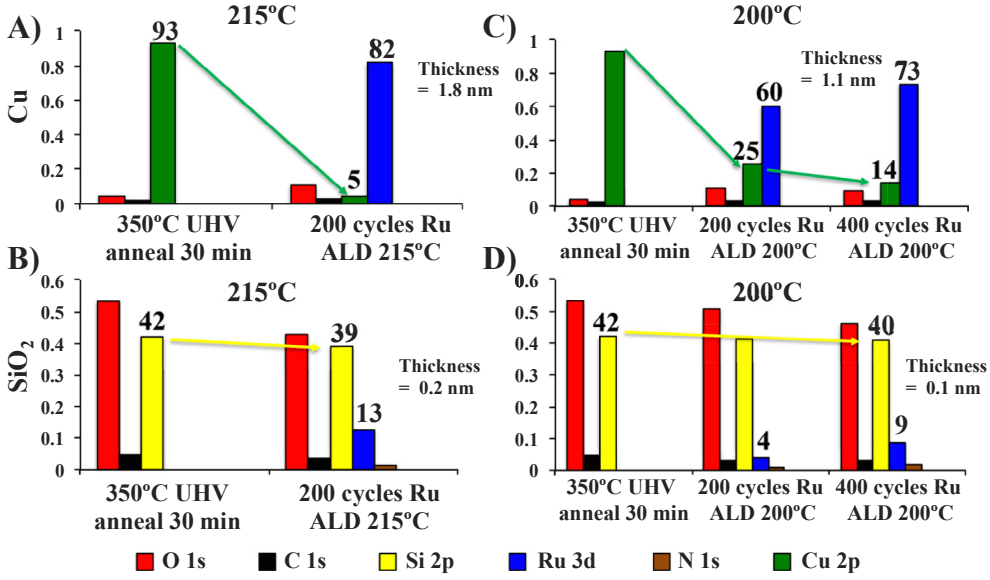

Fig. 10. Ru XPS on Cu vs SiO_2. At 215 °C, the selectivity of Ru ALD was 1.8 nm on (A) Cu (green arrows) vs. 0.2 nm on (B) SiO_2 (yellow arrows). Lowering the temperature slightly to 200 °C improved the selectivity on (C) Cu vs (D) SiO_2, but decreased the growth rate almost a factor of four. (For interpretation of the references to colour in this figure legend, the reader is referred to the web version of this article.)

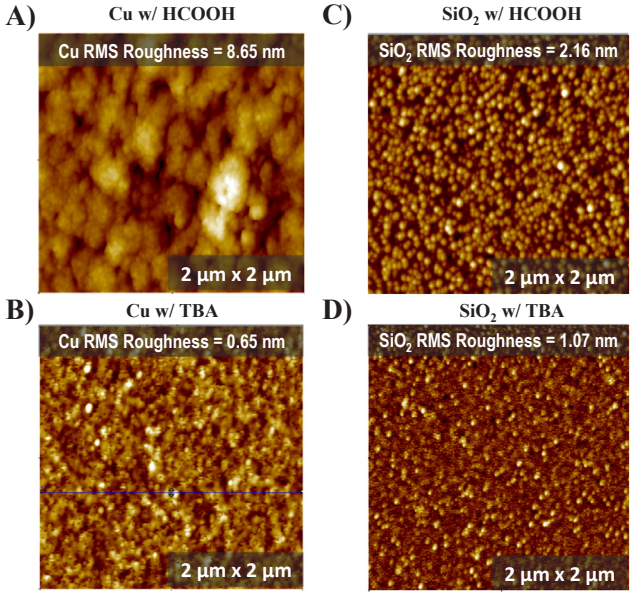

Fig. 11. Ru AFM on Cu with HCOOH and TBA. Much higher RMS surface roughness was observed from Ru ALD grown with (A) HCOOH compared to (B) TBA on Cu. Corresponding AFM of Ru grown on SiO_2 using (C) HCOOH and (D) TBA indicated the RMS surface roughness improved on Cu and SiO_2 by switching to TBA as a co-reactant.

as observed with the Co ALD process allows for the conclusion that more oxidized Ru ultimately would need to be deposited on SiO_2 to gain additional selectivity. It should also be noted that there is a small C 1s overlap with the Ru $3d_{3/2}$ component.

5. Discussion and conclusion

The mechanism of selectivity between the Co and Ru processes has been studied with XPS. For Co ALD, XPS saturation studies with HCOOH and TBA indicate a ligand exchange mechanism. As shown in Fig. 5 dosing HCOOH clearly increased the C, O, and shifted higher BE components of C and Co on the surface. Ending with a $Co(dad)_2$ pulse removes the higher BE formate on the surface inducing the formation of a volatile reaction byproduct. This was consistent with $Co(dad)_2$ promoting the dissociation of the formate ligand from the surface and ultimately driving the formation of a volatile specie(s) that are pumped away. In a similar manner, when TBA was used as a co-reactant, the C and N increase after TBA dosing, and were reduced after $Co(dad)_2$ dosing (supplemental material). This reaction was again consistent with a ligand exchange reaction occurring on the surface (Fig. 13).

As for the Ru ALD process, a slightly different mechanism is thought to occur due to inherent differences with the precursor being low valent and processing dissimilar ligands. When the $RuDMBD(CO)_3$ is introduced to the surface, the CO termination remains intact, but the weakly bound butadiene is able to dissociate and pump away. When the TBA is then introduced to the surface, the amine can react with the carbonyls inducing the formation of a volatile reaction byproduct that leaves the surface terminated with metallic Ru (Fig. 14).

The Co process is inherently more selective than the Ru process because of the formation of a very oxygen-rich CoO_x. The peak position between metallic Co grown on Pt/Cu and the oxidized Co grown on SiO_2 was nearly 4 eV with TBA. With HCOOH grown Co ALD, no CoO_x nuclei are hypothesized to have formed on SiO_2 due to likely etching by the HCOOH. In comparison, the Ru grown on Pt/Cu vs. SiO_2 was only 0.5 eV. This small difference means the sub-oxide of Ru is likely still conductive and able to continue the ALD reaction. Two factors are hypothesized to result in the lack of more oxygen-rich RuO_x formation: (a) The Ru precursor is low valent and (b) RuO_4 and even RuO_2 have heats of formation of −239 kJ/mol [28] and −315 kJ/mol [29], respectively, per Ru atom. Co_3O_4 has a heat of formation of −910 kJ/mol [30] that corresponds to −455 kJ/mol per Co atom. Therefore Co has a much stronger tendency to react with more weakly bound, under-coordinated oxygen on SiO_2. In order to achieve better selectivity, formation of a more oxygen-rich RuO_x is necessary consistent with the higher selectivity observed when using a Ru precursor, which has a Ru:O ratio of 4 such as dicarbonyl-bis(5-methyl-2,4-hexanediketonato) Ru [17]. Similarly, RuO_4, as fairly recently used by Minjauw *et al.* [31], may display improved selectivity.

The novel Ru ALD selectivity was limited due to the formation of a sub-stoichiometric RuO_x that was not as inhibitive to further deposition. To further improve the selectivity on Cu, use of oxygen-rich Ru precursor is needed since an oxidizing co-reactant must be avoided for interconnects. Hyper-selective Co metal deposition was produced from $Co(dad)_2$ and both co-reactants (HCOOH and TBA). Utilizing HCOOH, no deposition was seen on SiO_2 consistent with infinite deposition, however HCOOH was observed to etch Cu. By switching to TBA, no Cu etching was observed, a crucial restraint to be compatible with existing MEOL and BEOL processing, and similar metallic Co films were

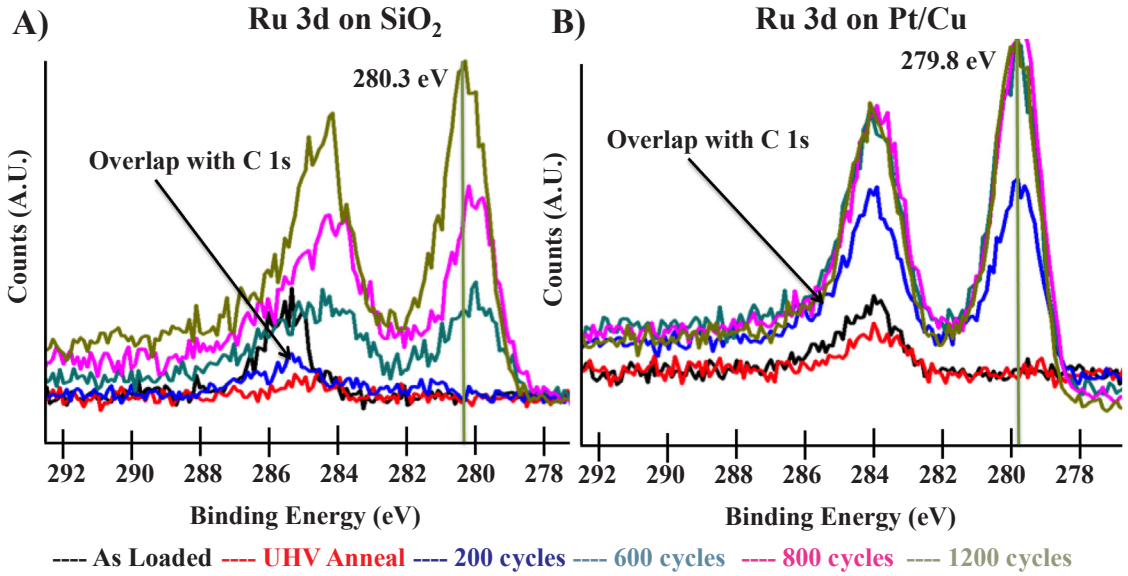

Fig. 12. Ru 3d raw XPS peaks. XPS peaks from the as loaded surfaces, after a UHV anneal, and after Ru ALD. The chemical shift of Ru grown on (A) SiO_2 vs (B) metallic substrates was only about 0.5 eV. This was consistent with a sub-stoichiometric RuO_x depositing on the surface unable to fully inhibit further Ru deposition. Note the small C 1 s overlap.

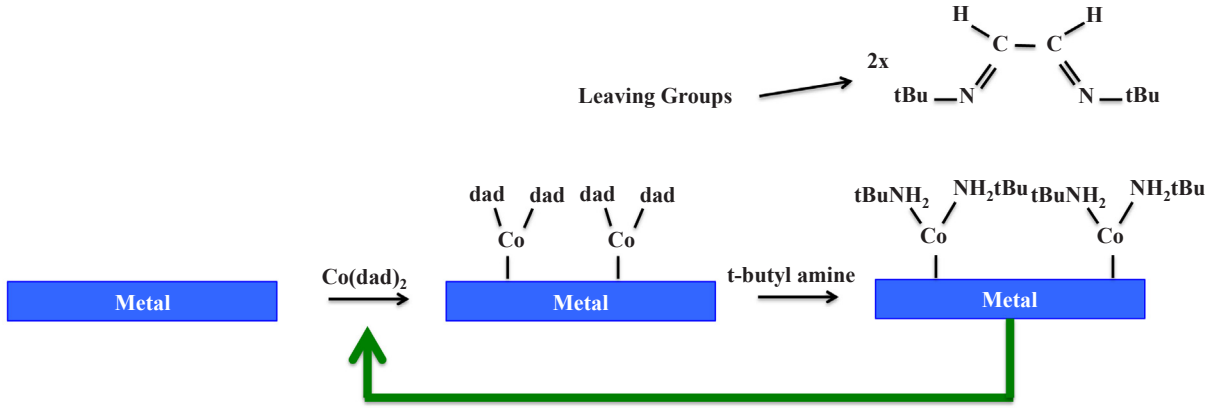

Fig. 13. Proposed mechanism for $Co(dad)_2$ + TBA ALD. When $Co(dad)_2$ is exposed to the surface, dad ligands terminate the surface. Following a dose with TBA, the dad ligands are replaced with the amine. The XPS data is consistent with ligand exchange.

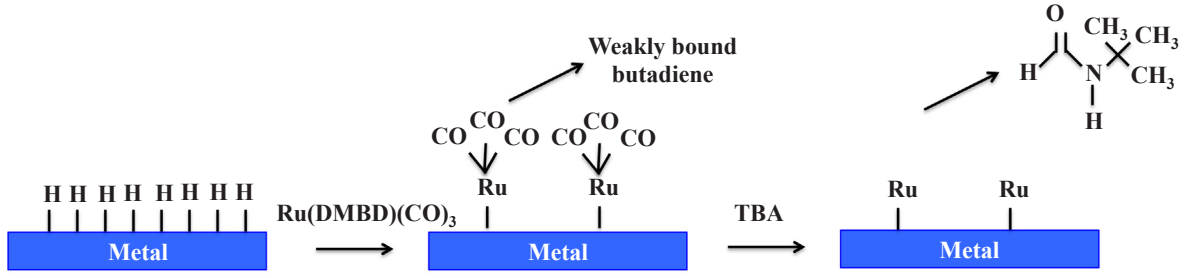

Fig. 14. Proposed mechanism for $RuDMBD(CO)_3$ + TBA ALD. When $RuDMBD(CO)_3$ was exposed to the surface the weakly bound butadiene was able to dissociate and volatilize. Following a dose with TBA, the CO ligands were able to react and induce a favorable reaction byproduct leaving metallic Ru on the surface.

deposited with only 4% CoO_x on SiO_2 independent of the number of Co ALD cycles. The self-limiting deposition on SiO_2 is a novel mechanism of selectivity through the formation of an oxidic particulate, which results in hyper-selectivity.

CRediT authorship contribution statement

Steven Wolf: Investigation, Methodology, Writing - review & editing. **Michael Breeden:** Investigation, Writing - review & editing. **Scott Ueda:** Investigation, Writing - review & editing. **Jacob Woodruff:** Conceptualization, Writing - review & editing. **Mansour Moinpour:** Conceptualization, Writing - review & editing. **Ravindra Kanjolia:** Conceptualization, Writing - review & editing. **Andrew Kummel:** Conceptualization, Supervision, Writing - review & editing.

Declaration of Competing Interest

The authors declare that they have no known competing financial interests or personal relationships that could have appeared to influence the work reported in this paper.

Acknowledgments

This work was performed in part at the San Diego Nanotechnology Infrastructure (SDNI) of UCSD, a member of the National Nanotechnology Coordinated Infrastructure, which is supported by the National Science Foundation (Grant ECCS-1542148) and by ASCENT, a Semiconductor Research Corporation (SRC) program. The authors gratefully acknowledge the valuable support of the SRC, Applied Materials who supplied the patterned sample, and EMD who provided the $RuDMBD(CO)_3$ precursor.

Appendix A. Supplementary material

Supplementary data to this article can be found online at https://doi.org/10.1016/j.apsusc.2019.144804.

References

[1] F. Chen, D. Gardner, Influence of line dimensions on the resistance of Cu interconnections, IEEE Electron Device Lett. 19 (1998) 508–510.
[2] J. Chawla, F. Gstrein, K. O'Brien, J. Clarke, D. Gall, Electron scattering at surfaces and grain boundaries in Cu thin films and wires, Phys. Rev. B 84 (2011) 235423.
[3] B. Feldman, S. Park, M. Haverty, S. Shankar, S.T. Dunham, Simulation of grain boundary effects on electronic transport in metals, and detailed causes of scattering, Physica Status Solidi (b) 247 (2010) 1791–1796.
[4] N. Bekiaris, et al., in 2017 IEEE International Interconnect Technology Conference (IITC), IEEE, 2017, pp. 1–3.
[5] L.G. Wen, et al., Atomic layer deposition of ruthenium with TiN interface for sub-10 nm advanced interconnects beyond copper, ACS Appl. Mater. Interfaces 8 (2016) 26119–26125.
[6] C.-C. Yang, P. Flaitz, P.-C. Wang, F. Chen, D. Edelstein, Characterization of selectively deposited cobalt capping layers: Selectivity and electromigration resistance, IEEE Electron. Device Lett. 31 (2010) 728–730.
[7] D. Gall, Electron mean free path in elemental metals, J. Appl. Phys. 119 (2016) 085101.
[8] R. Carpio, A. Jaworski, Management of copper damascene plating, J. Electrochem. Soc. 166 (2019) D3072–D3096.
[9] J.P. Klesko, M.M. Kerrigan, C.H. Winter, Low temperature thermal atomic layer deposition of cobalt metal films, Chem. Mater. 28 (2016) 700–703.
[10] M.M. Kerrigan, et al., Substrate selectivity in the low temperature atomic layer deposition of cobalt metal films from bis (1, 4-di-tert-butyl-1, 3-diazadienyl) cobalt and formic acid, J. Chem. Phys. 146 (2017) 052813.
[11] J. Kim, et al., Low-temperature atomic layer deposition of cobalt oxide as an effective catalyst for photoelectrochemical water-splitting devices, Chem. Mater. 29 (2017) 5796–5805.
[12] M.E. Alnes, E. Monakhov, H. Fjellvåg, O. Nilsen, Atomic layer deposition of copper oxide using copper (II) acetylacetonate and ozone, Chem. Vap. Deposition 18 (2012) 173–178.
[13] T. Aastrup, M. Wadsak, C. Leygraf, M. Schreiner, In situ studies of the initial atmospheric corrosion of copper influence of humidity, sulfur dioxide, ozone, and nitrogen dioxide, J. Electrochem. Soc. 147 (2000) 2543–2551.
[14] D.Z. Austin, et al., Atomic layer deposition of ruthenium and ruthenium oxide using a zero-oxidation state precursor, Chem. Mater. 29 (2017) 1107–1115.
[15] M.H. Hayes, C.L. Dezelah, J.F. Conley, Properties of annealed atomic-layer-deposited ruthenium from Ru (DMBD)(CO) 3 and oxygen, ECS Trans. 85 (2018) 743–749.
[16] Z. Gao, et al., Self-catalyzed, low-temperature atomic layer deposition of ruthenium metal using zero-valent, Ru (DMBD)(CO) 3 and water, Chem. Mater. (2019).
[17] R. Khan, et al., Area-selective atomic layer deposition using Si precursors as inhibitors, Chem. Mater. 30 (2018) 7603–7610.
[18] C. Powell, Recommended Auger parameters for 42 elemental solids, J. Electron Spectrosc. Relat. Phenom. 185 (2012) 1–3.
[19] N. McIntyre, M. Cook, X-ray photoelectron studies on some oxides and hydroxides of cobalt, nickel, and copper, Anal. Chem. 47 (1975) 2208–2213.
[20] E. Cano, C. Torres, J. Bastidas, An XPS study of copper corrosion originated by formic acid vapour at 40% and 80% relative humidity, Mater. Corros. 52 (2001) 667–676.
[21] W. Yang, H. Shintani, M. Akaike, T. Suga, in 2011 12th International Conference on Electronic Packaging Technology and High Density Packaging, IEEE, 2011, pp. 1–4.
[22] N. McIntyre, D. Johnston, L. Coatsworth, R. Davidson, J. Brown, X-ray photoelectron spectroscopic studies of thin film oxides of cobalt and molybdenum, Surf. Interface Anal. 15 (1990) 265–272.
[23] G. Carson, M. Nassir, M. Langell, Epitaxial growth of Co3O4 on CoO (100), J. Vacuum Sci. Technol. A: Vacuum, Surf. Films 14 (1996) 1637–1642.
[24] J. Fuggle, T. Madey, M. Steinkilberg, D. Menzel, Photoelectron spectroscopic studies of adsorption of CO and oxygen on Ru (001), Surf. Sci. 52 (1975) 521–541.
[25] C.S. Huang, M. Houalla, D.M. Hercules, C.L. Kibby, L. Petrakis, Comparison of catalysts derived from oxidation of ruthenium-thorium (Ru3Th7) with impregnated ruthenium/thoria catalysts, J. Phys. Chem. 93 (1989) 4540–4544.
[26] K. Kim, N. Winograd, X-ray photoelectron spectroscopic studies of ruthenium-oxygen surfaces, J. Catal. 35 (1974) 66–72.
[27] J. Shen, A. Adnot, S. Kaliaguine, An ESCA study of the interaction of oxygen with the surface of ruthenium, Appl. Surf. Sci. 51 (1991) 47–60.
[28] E. Mercer, D. Farrar, Heats of formation of RuO4, $RuO4^{-}$, and related compounds, Can. J. Chem. 47 (1969) 581–586.
[29] H.S.C. O'Neill, J. Nell, Gibbs free energies of formation of RuO 2, IrO 2, and OsO 2: A high-temperature electrochemical and calorimetric study, Geochim. Cosmochim. Acta 61 (1997) 5279–5293.
[30] M.W. Chase, et al., JANAF thermochemical tables, 1974 supplement, J. Phys. Chem. Ref. Data 3 (1974) 311–480.
[31] M.M. Minjauw, J. Dendooven, B. Capon, M. Schaekers, C. Detavernier, Atomic layer deposition of ruthenium at 100° C using the RuO 4-precursor and H 2, J. Mater. Chem. C 3 (2015) 132–137.